JPhys Materials

The role of pinhole structures in Mo thin films on multi-layer graphene synthesis

JPhys Materials

PAPER

The role of pinhole structures in Mo thin films on multi-layer graphene synthesis

Seda Kizir[1], **Wesley van den Beld**[1], **Bart Schurink**[1], **Robbert van de Kruijs**[1], **Jos Benschop**[1,2] and **Fred Bijkerk**[1]

[1] Industrial Focus Group XUV Optics, MESA + Institute of Nanotechnology, University of Twente, Enschede, The Netherlands
[2] ASML Netherlands B.V., Veldhoven, The Netherlands

E-mail: s.kizir@utwente.nl

Keywords: graphene, nucleation, pinhole, molybdenum carbide, density

OPEN ACCESS

RECEIVED
2 December 2019

REVISED
15 January 2020

ACCEPTED FOR PUBLICATION
24 January 2020

PUBLISHED
12 March 2020

Abstract

In this study, the density and oxygen content of Mo thin films were varied by changing the deposition conditions, in order to understand their influence on the catalytic activity of Mo_2C for the synthesis of multi-layer graphene (MLG). Structural and morphological analysis of Mo_2C in relation to its catalytic activity indicate that the density of Mo plays a more critical role on MLG synthesis than the oxygen content. Results show that the pinholes present in relatively low density Mo layers act as catalytically active defect sites, promoting MLG synthesis.

1. Introduction

Graphene has suitable properties for various application areas such as transparent conductors, transistors and sensors [1–4]. For industrially applicable wafer-scale graphene synthesis, chemical vapour deposition (CVD) is generally considered as the most promising method [5, 6].

Recently, transition metal carbides (TMC) have attracted the attention for enabling uniform graphene synthesis via CVD from single to multi-layers [7]. During such a CVD process, a stable carbide structure is formed from a parent metal, in the presence of a carbon source at elevated temperatures. In turn, this carbide serves as a catalyst for graphene synthesis. Unlike carbon soluble metals, carbide formation limits the carbon back diffusion from the catalyst upon cooling resulting in uniform graphene synthesis [7–9]. Mo_2C is a widely used catalyst among TMCs over the years for hydrogenation, water gas shift and methane reforming reactions due to its noble metal like catalytic activity, high temperature resistance and low cost [10–13] but the use of Mo_2C on graphene synthesis is a relatively recent development [7, 14–16]. Literature studies mainly focus on Mo_2C and graphene synthesis using Mo foils, which are expected to possess a different structure and morphology compared to Mo thin films.

Graphene synthesis using thin film catalysts via a CVD process is important for scalability for industrial applications. The graphene synthesis mechanism is determined by various factors such as the crystallinity of the catalyst, the crystalline planes present on the catalyst surface and surface imperfections of the catalyst in the form of defects (e.g. grain boundaries, step sites, terraces and kink sites) [17–23]. Therefore, it is crucial to understand how Mo thin film properties influence the development of the Mo_2C thin film structure and morphology which in turn affect the catalytic activity for graphene synthesis.

Mo thin film properties, such as density and oxygen content, are known to change with respect to deposition conditions [24, 25]. The variation of density values of Mo layers, from close to bulk density to porous Mo layers, heavily impacts Mo layer microstructure and morphology [24]. In addition, literature shows that adding oxygen gas upon deposition of the Mo layer causes micro structural changes [26].

In this study, we show that the influence of the oxygen content and density on the surface morphology of a Mo_2C catalyst, in particular defect formation mechanism such as pinholes, play an important role in synthesis of multi-layer graphene (MLG).

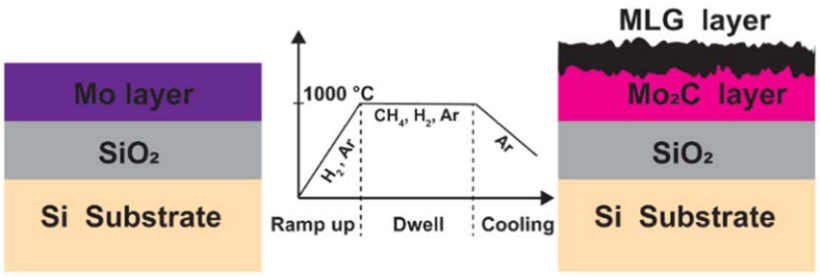

Figure 1. The CVD process involves three steps: ramp up to the process temperature in H_2 and Ar, dwell in CH_4, H_2 and Ar, and cooling in Ar. The result of this full process is that a Mo layer transforms to Mo_2C and multi-layer graphene is deposited on its surface.

Table 1. Overview of the system parameters of the four Mo deposition techniques.

Mo layers	Base pressure	Sputter pressure	Target to substrate distance	Sputter voltage
System 1 Sputtering	10^{-8} mbar	10^{-3} mbar	300 mm	366–382 V
System 2 Sputtering	10^{-7} mbar	6.6×10^{-3} mbar	145 mm	253–259 V
System 3 E-gun	10^{-9} mbar	—	—	—
System 4 E-gun	10^{-8} mbar	—	—	—

2. Experimental methods

A 300 nm SiO_2 diffusion barrier layer is deposited on a single-side polished Si (100) wafer, followed by the deposition of 70 nm thick Mo layer. Note that the wafers are cleaned with HNO_3 for 5 min prior to Mo deposition to remove organic contaminants. The Mo layers are deposited using four different coating systems, two sputter systems and two e-gun evaporation systems. Argon gas is used for the Mo sputtering process, and for additional experiments oxygen gas is added. The details of the deposition conditions used in all four systems are given in table 1.

For CVD depositions, a cold wall reactor system is used. In figure 1, the CVD process is described in three steps as ramp up, dwell and cooling within the CVD recipe. First, Mo layers on SiO_2/Si substrates are annealed up to 1000 °C during the ramp up step in H_2 and Ar environment to remove the native oxide on the Mo layer. After opening the CH_4, the Mo layer is converted to Mo_2C catalyst, initiating the MLG synthesis during the dwell step. Next, samples are fast cooled in order to minimize the back diffusion of carbon from Mo_2C for uniform deposition of MLG. It should be noted that except variation in Mo layer deposition conditions, all other parameters were kept unchanged throughout the study.

Raman spectroscopy is performed for analyzing the graphene synthesized on the Mo_2C surface. Raman measurements are carried out with a WITec alpha 300 system using a 532 nm laser (1 mW) and a 100× objective (0.9 NA). The Raman spectra have been averaged over a 10 μm × 10 μm scan area. The crystallinity and structure of Mo_2C layers are studied using grazing incidence x-ray diffraction measurements (GIXRD). X-ray reflectivity (XRR) measurements are used to determine the density of the Mo layers. GIXRD and XRR measurements are performed using Panalytical Empyrean systems with a Cu-$K\alpha$ source (0.154 nm). The Mo layer oxygen content is evaluated by x-ray photoelectron spectroscopy (XPS) depth profiling using Thermo Theta probe spectrometer (monochromatic Al-$K\alpha$ radiation (1486.6 eV) with a spot size of 200 μm) and Ar^+ ion gun with acceleration voltage of 500 V. Prior to the analysis, possible organic contaminants and native oxide on top of the Mo layer are removed using Ar^+ ion gun etching. Subsequent recurrent etching steps are performed to determine an average value of oxygen content throughout the layer. The XPS data is fitted using the Thermo Scientific Avantage software. Characterization of surface topography is performed using scanning electron microscopy (SEM) and crystalline planes of the surfaces are determined by electron backscatter diffraction (EBSD), both recorded by a Zeiss MERLIN HR-SEM system. SEM measurements are carried out at a voltage of 1.4 kV. EBSD measurements are performed using an acceleration voltage of 20 kV with a specimen tilt of 70°. It should be noted that samples are not polished prior to EBSD measurements in order to avoid any sample preparation induced damages.

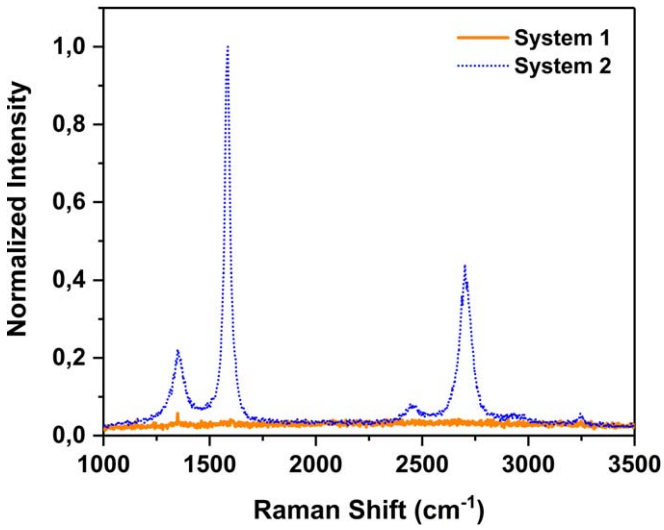

Figure 2. Raman spectra show the presence of graphene on Mo_2C after CVD processing of a Mo layer from System 2, whereas graphene peaks are absent on Mo_2C after CVD of Mo from System 1 using the same CVD conditions.

3. Results and discussion

The basis of this study relates to the properties of the deposited Mo layer, as in density and oxygen content, and its behaviour in the the transition to Mo_2C for the growth of graphene in the CVD process. To deposit these Mo thin films, two different magnetron sputtering (Systems 1, 2) and two different e-gun systems (Systems 3, 4) are used, as given in table 1. Magnetron sputtering is selected due to the flexibility in changing the density of the deposited layer (depending on sputter energies) and oxygen parameters (by adding oxygen gas during Mo deposition). However, magnetron sputtering does not allow for deposition of low density Mo layers with a low oxygen content. A reduction sputter energy towards low density also reduces the deposition rate and thus increases the inclusion oxygen. Hence, e-gun evaporation is selected for the deposition of Mo layers with both a low density and a low oxygen content.

The different Mo layers will undergo the standard CVD process as indicated, and the outcome in terms of MLG growth is investigated. The results will be presented here in two parts.

In the first part, sputter deposited Mo layers from Systems 1 and 2 are tested for CVD processing. Raman spectra revealed that only Mo layers from System 2 result in graphene synthesis. In order to understand this remarkable difference in catalytic activity of Mo_2C layers, both as-deposited Mo layers (before CVD) and the Mo_2C layers after CVD are studied in detail. To investigate the effect of Mo_2C catalyst crystallinity, GIXRD and EBSD measurements are performed. Mo layers are characterized with XPS and XRR to determine the oxygen content and density values respectively.

In the second part, the influence of density and oxygen content will be further explored in more detail by investigating the additional Mo layers deposited by Systems 3 and 4 to broaden the spectrum. Their impact on the surface morphology of Mo_2C leading to MLG growth (after CVD) has been studied extensively by XPS, XRR, Raman and SEM, respectively.

3.1. Effect of sputtering of Mo layer on MLG synthesis

The Raman mapping of graphene on Mo_2C layers after CVD process which are synthesized using Mo layers from sputtering Systems 1 and 2 are shown in figure 2. The Raman spectra indicates the characteristic peaks of graphene on Mo_2C from System 2: the peaks at 1357 cm^{-1}, 1590 cm^{-1} and 2709 cm^{-1}, represent the D peak, G peak and 2D peak, respectively, and the additional peaks represents the overtone peaks (~2400, ~2900 and ~3250 cm^{-1}). Relative intensity ratio of 2D peak to G peak is found as 0.36, and the full width half maximum value of 2D peak is found as 48 cm^{-1}, indicating MLG synthesis [27], which is expected for Mo thin films [7]. The relative intensity ratio of D peak to G peak (Id/Ig ratio) is calculated to be 0.17. This suggest that graphene is significantly less disordered in terms of e.g. grain boundaries when compared to graphene grown on Mo foils with a typical Id/Ig ratio of ~0.9 [15]. This is attributed to the possible structural and morphological differences between Mo_2C thin films and the Mo foils.

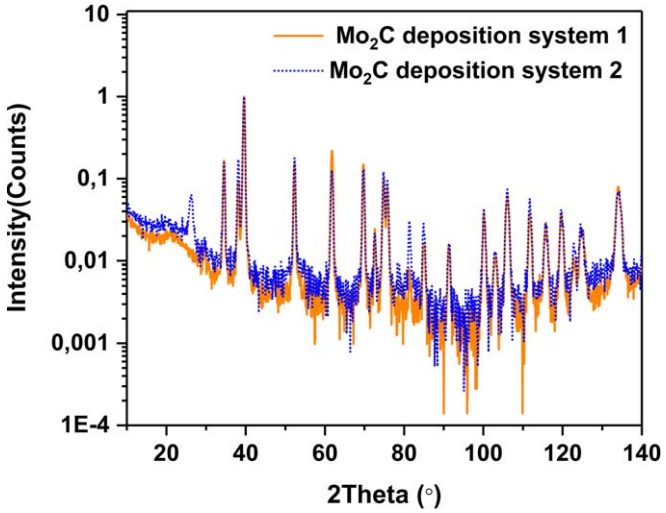

Figure 3. GIXRD measurements indicate comparable crystallinity of Mo_2C layers from the two different systems. The additional peak at 26° corresponds to the MLG peak on the Mo_2C layer from System 2.

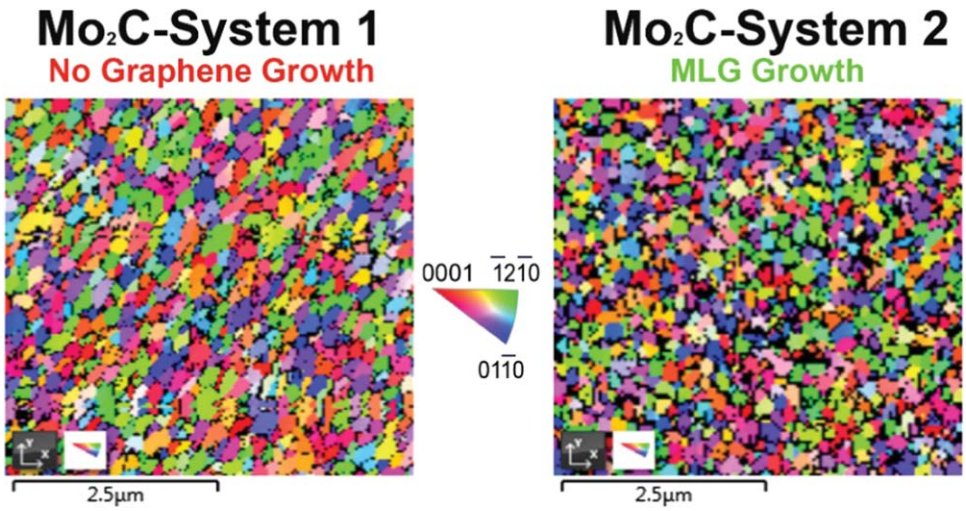

Figure 4. EBSD analysis showing the crystalline planes on the surface of the Mo_2C layers. Crystalline planes are randomly oriented for Mo_2C structures originating from sputter deposition Systems 1 and 2.

3.2. Mo_2C crystallinity

The finding that the Mo layer from System 2 allows for MLG growth is further investigated. The difference in deposition between Systems 1 and 2 hints toward a difference in the film crystallinity. It has been reported that catalytic activity of Mo_2C can be sensitive to its crystalline structure depending on whether the α-Mo_2C (cubic phase) or β-Mo_2C (hexagonal phase) form is present [28, 29]. This structure dependence can also effect the catalytic activity for graphene synthesis. Therefore, GIXRD measurements are performed to identify the crystalline structure of the prepared Mo_2C layers. GIXRD spectra of Mo_2C layers after CVD from Systems 1 and 2 can be found in figure 3. Results show overlapping spectra of similar hexagonal Mo_2C structures with reference code (NIST pattern, 03-065-8766) for the two sputtering systems. Furthermore, no shift in Mo_2C peak positions is observed indicating similar structures with no additional phase impurities or strain. Moreover, at 26° the MLG (002) peak is observed on Mo_2C from System 2 (reference code: NIST pattern, 03-065-6212). Nevertheless, it is important to realize that the, crystalline orientations on the surface can be different compared to bulk crystallinity, which can potentially result in differences in catalytic activity. In order to verify the surface orientations, Mo_2C have been analysed with EBSD. The EBSD result, shown in figure 4, confirms that similar randomly oriented crystalline planes are present at the surface for both the Mo_2C layers.

Considering the fact that MLG is observed only on the Mo_2C layer prepared from the Mo layer deposited using System 2, while the GIXRD spectra (figure 3) and EBSD measurements (figure 4) are comparable for both

Mo_2C layers, it is concluded that the crystallinity cannot explain the observed difference in catalytic activity of the Mo_2C layers prepared by Systems 1 and 2. Yet the EBSD images show a significant difference in 'dark areas' between the Mo_2C layers obtained from the Mo depositions in Systems 1 and 2. The 'dark areas' in the EBSD analysis indicate the presence of morphology related defect sites on surface, which might again be the influence of the Mo oxygen content and density before CVD. To further unravel this relation, the exact values of the density and oxygen content measured.

3.3. Density and oxygen content of Mo layers

The density of both the as-deposited Mo layers (before CVD) has been analyzed using XRR. Mo layers deposited by System 1 shows a high density around 10.2 g cm^{-3} (close to bulk Mo density of 10.28 g cm^{-3}) in contrast to the Mo layers from System 2 with a lower density value of around 8.8 g cm^{-3}. The difference in density of these Mo layers can be explained by a different target to substrate distance used in both sputter system designs which results in a different number of collisions of the sputtered atoms before they arrive at the substrate. Also, the deposition voltages and sputter pressures are different for both systems which can result in a difference in deposition energy. To put this in perspective, an estimate for the average number of collisions in both sputter systems is made by dividing the substrate to target distance to the mean free path at the used sputter pressures. This calculation shows that System 2 has around 3 times higher average number of collisions compared to System 1 which causes the deposition energy to be significant lower. Therefore, the average energy of the deposited Mo atoms is relatively lower in System 2 when compared to System 2, which typically leads to the formation of more defect sites during deposition.

For the oxygen content, the as-deposited Mo layers are investigated further using XPS. The XPS analysis shows that System 2 Mo layer has 8%–11% of O/Mo ratio while Mo layer from System 1 has 0.1% O/Mo ratio. There are two factors which can commonly affect the oxygen content of Mo layers: base pressure and deposition rate. The base pressure of System 2 is a factor 10 higher when compared to System 1, which results in more oxidation during deposition. Deposition rates for both sputter systems is similar (System 1: 0.174 nm s^{-1}, System 2: 0.164 nm s^{-1}) and is not expected to give rise to significant oxidation.

The finding that Mo layer from System 2 allows for MLG growth and the Mo layer from System 1 results in no MLG growth is further studied. The suspecting difference in density and oxygen content of the Mo layers has no significant effect on the crystallinity leading to the difference in MLG growth. In the next section, density and oxygen content of Mo layers are investigated in more detail to understand the dominating effect resulting in the dramatic change in catalytic activity of Mo_2C thin films for MLG synthesis.

3.4. Effect of density and oxygen content of Mo layers on MLG synthesis

The effect of density and oxygen content of Mo layers on MLG synthesis is studied by varying sputter deposition parameters of System 1, to observe the effect on catalytic activity for graphene synthesis. Here the sputter pressure is increased, which generally reduces the density values of the deposited layers [24]. First, the sputter pressure is increased to lower the deposition energy, in order to achieve a relatively low density Mo layers. Second, oxygen gas is added during deposition of the Mo layers to increase the oxygen content of the as-deposited Mo layers. In addition, lower sputtering energies are generally known to cause more oxygen incorporation to Mo layers due to lower deposition rate. To obtain relatively low density Mo layers with a low oxygen content, Mo layers are also deposited using e-gun evaporation. Since evaporation is a low energy deposition technique, these layers are expected to have a low density in combination with a low oxygen content. Therefore, to investigate the impact of density and oxygen further, layers have been deposited with varying composition by using the four Mo deposition systems (Systems 1–4).

An overview of the analysis results from the four different systems (two sputtering and two e-gun evaporation) is shown in figure 5. The presence of MLG after the CVD process, observed in Raman spectra, is plotted as function of both the initial density and oxygen content of as-deposited Mo layers (before CVD). As discussed before, density values of the Mo films are extracted from XRR fits and the O/Mo ratios are obtained from XPS depth profile analysis. When the initial Mo density is close to the bulk value of Mo (System 1), MLG synthesis is not observed, independent from the oxygen content. For lower Mo layer densities, MLG synthesis is typically obtained, with a minor influence of the oxygen content. Therefore it is concluded that the density of the Mo layers is playing a dominant role on MLG synthesis as compared to the oxygen content.

To study the role of the as-deposited Mo layer density on creating a catalytically active surface morphology for Mo_2C layers, the initial oxygen content of Mo layers should be kept constant while varying the density. For this reason, two samples have been selected with an O/Mo ratio of about 8% from sputtering Systems 1 and 2 and represented by an arrow in figure 5.

These Mo_2C layers from Systems 1 and 2 with similar oxygen content (figure 5, arrow) are imaged by SEM, to examine the surface morphology, especially the presence of defect sites. Since the conductive MLG, covering the

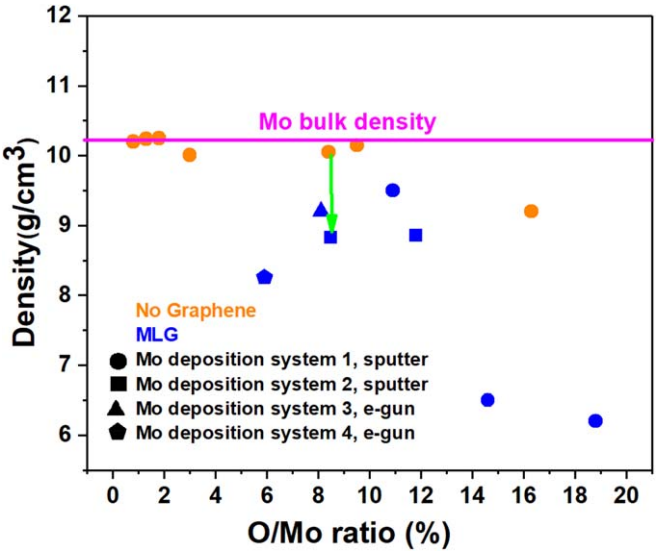

Figure 5. MLG synthesis after CVD process is characterized by Raman measurements as a function of oxygen content and density. The presence of G, D and 2D peaks above noise level in Raman spectra is represented as graphene synthesis given by symbols with blue colour and no graphene synthesis is shown by symbols with orange colour. Oxygen content of Mo layers are measured via XPS and density values are extracted from XRR fits. Oxygen content of Mo layer from System 1 is increased by adding oxygen gas during deposition of Mo and density of Mo layer is reduced by increasing the sputtering pressure. Green arrow represents two samples in similar oxygen contents but different densities resulting in a drastic change on graphene synthesis.

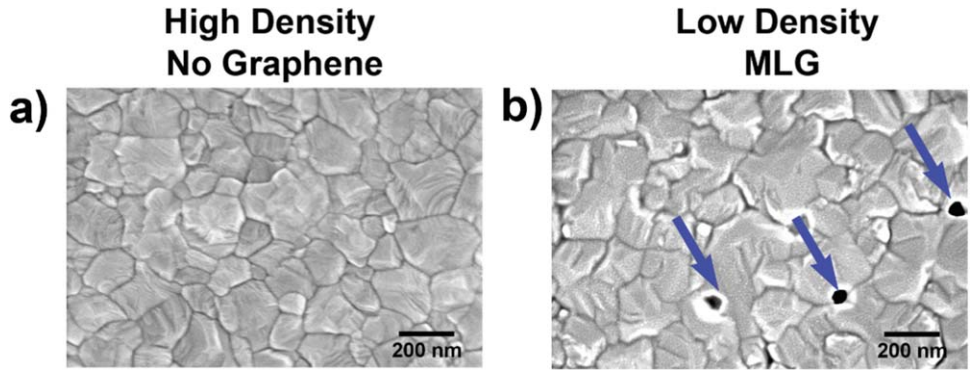

Figure 6. SEM images showing the morphology difference of Mo_2C layers (after CVD) from high density and low density deposited Mo layers for which a dramatic difference for graphene synthesis by CVD is observed. High density Mo layers after CVD show no pinholes and no graphene deposition (a), whereas low density Mo layers after CVD show pinhole defects (as indicated by the arrows) after MLG removal (b).

entire Mo_2C surface (as demonstrated in earlier work [30]), might change the image contrast in SEM, MLG is removed from the top of the Mo_2C layer (System 2) using a hydrogen plasma treatment. SEM images displayed in figure 6 reveal that defects in the form of pinholes are only present in the Mo_2C layer originating from System 2 and not in Mo_2C layer originating from System 1.

Pinholes are known to be catalytically active sites [31], which implies an increased reactivity at pinhole sites. In addition graphene synthesis is generally known to start with nucleation at defect sites, which have low energy barrier for nucleation [32]. Therefore, the difference in graphene synthesis is explained by the formation of pinholes as defect sites on Mo_2C layer as represented in figure 6.

The mechanism for the formation of defects is further investigated before Mo_2C formation to understand the link between density and pinhole formation, where pinholes are only observed in the low density Mo layers. It is stated in the literature that Mo layers are prone to cracking and eruption of pinholes upon development of stress during post annealing processes [33]. Furthermore, it has been reported that the initial deposition conditions of Mo are important for temperature induced failures, in particular porous Mo layers deposited at high sputter pressures, which are more prone to form defects [34].

Next, standard Mo layers from two different sputtering systems (Systems 1 and 2) are also investigated after ramp up step (annealing) to 1000 °C to observe the temperature induced pinholes prior to carbide formation.

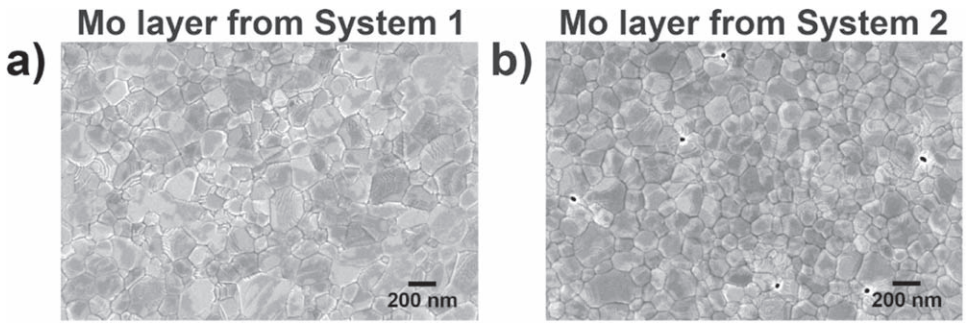

Figure 7. SEM measurements after ramp up process (annealing) on Mo layers showing (a) pinholes are visible for high density Mo layers whereas not visible for (b) low density Mo layers before graphene synthesis process.

Standard Mo layers from System 1 (without adding oxygen or increasing the sputter pressure) and System 2 are imaged via SEM after the first CVD step 'ramp up' (increasing the sample temperature in hydrogen) and subsequently pinholes are observed for Mo layers from System 2, whereas these defects are absent for the sample prepared by Mo from System 1 (figure 7).

4. Conclusion

The possible origin of MLG synthesis using Mo_2C template layers was investigated by focusing on the properties of the Mo template layers. We demonstrated, by a density and oxygen content analysis of the as-deposited Mo thin films, that the catalytic activity of Mo_2C for MLG synthesis is dramatically increased for Mo layers with densities below about 90% of the bulk density, whereas graphene synthesis is not possible for Mo densities close to the bulk value. It has been shown that the density of the Mo layers impacts the surface morphology of the Mo_2C. Defects in the form of pinholes are formed by low energy deposition of Mo layers and the subsequent formation of the Mo_2C during the CVD process which leads to MLG deposition. There are strong indications that the pinhole defects serve as catalytically active sites for nucleation of graphene which is potentially also relevant for other metals.

Acknowledgments

This research is part of Top Sector High Tech Systems and Materials Project 15357 of the Technology Foundation STW (nowaddays TTW), which is part of the Netherlands Organization for Scientific Research (NWO). It is co-funded by NWO and ASML (Veldhoven). The project is carried out in the Industrial Focus Group XUV Optics, supported by the University of Twente, ASML, Carl Zeiss SMT, Malvern Panalytical, as well as the Province of Overijssel. In addition, the authors thank Mark A Smithers for his assistance in performing the SEM measurements.

ORCID iDs

Seda Kizir https://orcid.org/0000-0001-7540-5318
Wesley van den Beld https://orcid.org/https://orcid.org/0000-0002-5449-3838
Fred Bijkerk https://orcid.org/https://orcid.org/0000-0002-0465-0241

References

[1] Zhong Y, Zhen Z and Zhu H 2017 Graphene: fundamental research and potential applications *FlatChem* **4** 20–32
[2] Klekachev A V *et al* 2013 Graphene transistors and photodetectors *Electrochem. Soc. Interface* **22** 63–8
[3] Mahmoudi T, Wang Y and Hahn Y B 2018 Graphene and its derivatives for solar cells application *Nano Energy* **47** 51–65
[4] Nag A, Mitra A and Mukhopadhyay S C 2018 Graphene and its sensor-based applications: a review *Sensors Actuators* A **270** 177–94
[5] Mattevi C, Kim H and Chhowalla M 2011 A review of chemical vapour deposition of graphene on copper *J. Mater. Chem.* **21** 3324–34
[6] Muñoz R and Gómez-Aleixandre C 2013 Review of CVD synthesis of graphene *Chem. Vapor Depos.* **19** 297–322
[7] Zou Z, Fu L, Song X, Zhang Y and Liu Z 2014 Carbide-forming groups IVB-VIB metals: a new territory in the periodic table for CVD growth of graphene *Nano Lett.* **14** 3832–9
[8] Seah C M, Chai S P and Mohamed A R 2014 Mechanisms of graphene growth by chemical vapour deposition on transition metals *Carbon* **70** 1–21

[9] Nakajima Y, Murata H, Saitoh N, Yoshizawa N, Suemasu T and Toko K 2018 Metal catalysts for layer-exchange growth of multilayer graphene *ACS Appl. Mater. Interfaces* **10** 41664–9
[10] Patt J, Moon D J, Phillips C and Thompson L 2000 Molybdenum carbide catalysts for water-gas shift *Catal. Lett.* **65** 193–5
[11] Lamont D C and Thomson W J 2005 Dry reforming kinetics over a bulk molybdenum carbide catalyst *Chem. Eng. Sci.* **60** 3553–9
[12] Dhandapani B St., Clair T and Oyama S T 1998 Simultaneous hydrodesulfurization, hydrodeoxygenation, and hydrogenation with molybdenum carbide *Appl. Catal.* A **168** 219–28
[13] Ma Y, Guan G, Hao X, Cao J and Abudula A 2017 Molybdenum carbide as alternative catalyst for hydrogen production—a review *Renew. Sustain. Energy Rev.* **75** 1101–29
[14] Wu Y *et al* 2012 Synthesis of large-area graphene on molybdenum foils by chemical vapor deposition *Carbon* **50** 5226–31
[15] Park S J, Jaleh B, Naghdi S, Kim M T and Rhee K Y 2016 Atmospheric chemical vapor deposition of graphene on molybdenum foil at different growth temperatures *Carbon Lett.* **18** 37–42
[16] Grachova Y, Vollebregt S, Lacaita A L and Sarro P M 2014 High quality wafer-scale CVD graphene on molybdenum thin film for sensing application *Procedia Eng.* **87** 1501–4
[17] Ishihara M, Koga Y, Kim J, Tsugawa K and Hasegawa M 2011 Direct evidence of advantage of Cu(111) for graphene synthesis by using raman mapping and electron backscatter diffraction *Mater. Lett.* **65** 2864–7
[18] Frank O, Vejpravova J, Holy V, Kavan L and Kalbac M 2014 Interaction between graphene and copper substrate: the role of lattice orientation *Carbon* **68** 440–51
[19] Gao J, Yip J, Zhao J, Yakobson B I and Ding F 2011 Graphene nucleation on transition metal surface: structure transformation and role of the metal step edge *J. Am. Chem. Soc.* **133** 5009–15
[20] Liu W, Li H, Xu C, Khatami Y and Banerjee K 2011 Synthesis of high-quality monolayer and bilayer graphene on copper using chemical vapor deposition *Carbon* **49** 4122–30
[21] Wofford J M, Nie S, McCarty K F, Bartelt N C and Dubon O D 2010 Graphene islands on Cu foils: the interplay between shape, orientation, and defects *Nano Lett.* **10** 4890–6
[22] Coraux J, N'Diaye A T, Busse C and Michely T 2008 Structural coherency of graphene on Ir(111) *Nano Lett.* **8** 565–70
[23] Calvo M R *et al* 2012 Activation energy paths for graphene nucleation and growth on Cu *ACS Nano* **6** 3614–23
[24] Li W, Yan X, Aberle A G and Venkataraj S 2015 Effect of deposition pressure on the properties of magnetron-sputter-deposited molybdenum back contacts for CIGS solar cells *Japan. J. Appl. Phys.* **54** O8KC14
[25] Bardin T T, Pronko J G, Budhani R C, Lin J S and Bunshah R F 1988 The effects of oxygen concentration in sputter-deposited molybdenum films *Thin Solid Films* **165** 243–7
[26] Pachlhofer J M *et al* 2017 Industrial-scale sputter deposition of molybdenum oxide thin films: microstructure evolution and properties *J. Vac. Sci. Technol.* A **35** 021504
[27] Ferrari A C *et al* 2006 Raman spectrum of graphene and graphene layers *Phys. Rev. Lett.* **97** 187401
[28] Souza Macedo L, Oliveira R R, van Haasterecht T, Teixeira da Silva V and Bitter H 2019 Influence of synthesis method on molybdenum carbide crystal structure and catalytic performance in stearic acid hydrodeoxygenation *Appl. Catal.* B **241** 81–8
[29] Qi K Z, Wang G C and Zheng W J 2013 A first-principles study of CO hydrogenation into methane on molybdenum carbides catalysts *Surf. Sci.* **614** 53–63
[30] Mund B K, Sturm J M, van den Beld W T E, Lee C J and Bijkerk F 2019 Etching processes of transferred and non-transferred multi-layer graphene in the presence of extreme UV, H_2O and H_2 *Appl. Surf. Sci.* **504** 144485
[31] Waterhouse G I N, Bowmaker G A and Metson J B 2004 Influence of catalyst morphology on the performance of electrolytic silver catalysts for the partial oxidation of methanol to formaldehyde *Appl. Catal.* A **266** 257–73
[32] Ani M H *et al* 2018 A critical review on the contributions of chemical and physical factors toward the nucleation and growth of large-area graphene *J. Mater. Sci.* **53** 7095–111
[33] Lin Y C, Yen W T and Wang L Q 2012 Effect of substrate temperature on the characterization of molybdenum contacts deposited by DC magnetron sputtering *Chin. J. Phys.* **50.1** 82–8
[34] Yoon J H *et al* 2011 High-temperature stability of molybdenum (Mo) back contacts for CIGS solar cells: a route towards more robust back contacts *J. Phys. D: Appl. Phys.* **44** 425302